

# Ultrasonic parametric imaging of erythrocyte aggregation using the structure factor size estimator \*

François T.H. Yu <sup>a</sup>, Émilie Franceschini <sup>a</sup>, Boris Chayer <sup>a</sup>, Jonathan K. Armstrong <sup>b</sup>, Herbert J. Meiselman <sup>b</sup> and Guy Cloutier <sup>a,c,\*\*</sup>

<sup>a</sup> *Laboratory of Biorheology and Medical Ultrasonics, Centre de Recherche, Centre Hospitalier de l'Université de Montréal, Montréal, QC, Canada*

<sup>b</sup> *Department of Physiology and Biophysics, Keck School of Medicine, University of Southern California, Los Angeles, CA, USA*

<sup>c</sup> *Department of Radiology, Radio-Oncology and Nuclear Medicine and Institute of Biomedical Engineering, Université de Montréal, Montréal, QC, Canada*

Received 7 January 2009

Accepted in revised form 25 June 2009

**Abstract.** Ultrasound characterization of erythrocyte aggregation (EA) is attractive because it is a non-invasive imaging modality that can be applied *in vivo* and *in situ*. An experimental validation of the Structure Factor Size Estimator (SFSE), a non-Rayleigh scattering model adapted for dense suspensions, was performed on 4 erythrocyte preparations with different aggregation tendencies. Erythrocyte preparations were circulated in Couette and tube flows while acoustically imaged over a bandwidth of 9–28 MHz. Two acoustically derived parameters, the packing factor ( $W$ ) and ensemble averaged aggregate size ( $D$ ), predictably increased with increasing EA, a finding corroborated by bulk viscosity measurements. In tube flow, a “black hole” reflecting the absence of aggregates was observed in the center stream of some parametric images. The SFSE clearly allowed quantifying the EA spatial distribution with larger aggregates closer to the tube walls as the aggregation tendency was increased. In Couette flow,  $W$  and  $D$  were uniformly distributed across the shear field. Assuming that the viscosity increase at low shear is mainly determined by EA, viscosity maps were computed in tube flow. Interestingly, erythrocyte suspensions with high aggregabilities resulted in homogeneous viscosity distributions, whereas a “normal” aggregability promoted the formation of concentric rings with varying viscosities.

**Keywords:** Ultrasound backscattering coefficient, ultrasound tissue characterization, packing factor, Born approximation, non-Rayleigh scattering, hemorheology, local viscosity

## 1. Introduction

Blood is a shear thinning non-Newtonian fluid: in steady state, the viscosity increase at low shear is predominantly caused by reversible erythrocyte aggregation (EA) [8]. The level of EA is dependent

---

\*This article is based on a paper given by Dr. Guy Cloutier in Symposium 31 at the 13th International Congress of Biorheology and 6th International Conference of Clinical Hemorheology at the Pennsylvania State University, State College, PA, USA, July 9–14, 2008.

\*\*Address for correspondence: Guy Cloutier, Director LBUM-CRCHUM, 2099 Alexandre de Sève, Pavillon J.A. de Sève (room Y-1619), Montréal, QC, H2L 2W5, Canada. Tel.: +1 514 890 8000 (24703); Fax: +1 514 412 7505; E-mail: guy.cloutier@umontreal.ca; URL: <http://lbum-crchum.com>.

on the erythrocyte aggregability [43], on the concentration of aggregation-inducing macromolecules in plasma (primarily fibrinogen but also immunoglobulins and other inflammatory proteins) and on mechanical shearing forces [3,9]. Indices of aggregation can be measured *in vitro* on samples obtained by venipuncture using different techniques – including viscosimetry, erythrocyte sedimentation rate, electrical impedance, light and ultrasound scattering [54]. In humans, increased bulk blood viscosity and aggregation measured *in vitro* correlate with numerous cardiovascular diseases and complications including diabetes [27,33], deep venous thrombosis and its recurrence [10,30], and ischemic heart events [32,61]. The fact that these diseases and their complications generally occur in specific locations of the vascular system suggest a pathological micro- and/or macro-circulatory hemodynamic contribution to their etiologies.

Analytical [18,42,45] and numerical [4,26,65] models have been proposed to interpret the rheological behavior of blood. However, the complexity of the time dependent non-Newtonian behavior of blood and the computational loads required for transposing numerical models to real vascular and erythrocyte geometries remain important challenges for these approaches. Ultrasound (US) imaging, which utilizes non-invasive pressure wave propagation through biological tissues, is a tool that has the potential to measure EA for both *in vivo* and *in situ* flow conditions. This imaging modality could significantly contribute to hemorheology especially at high US frequencies, since it allows characterization of EA in space and in time, as demonstrated by its sensitivity to measure aggregate formation kinetics [11, 14] and its ability to follow cyclic aggregation and disaggregation states under pulsatile flows [17,39]. *In situ* quantification, etiological impacts and *in vivo* monitoring are potential applications of US EA characterization.

### 1.1. Ultrasound and EA

The increased B-mode blood echogenicity caused by EA during clinical scans, typically performed at 2–12 MHz, is well known [28,52]. The access to radio-frequency (RF) data from laboratory instruments and, increasingly, from clinical scanners allows application of a normalization procedure [34,53,58] to obtain a backscattering coefficient (BSC), defined as the power backscattered by a unit volume of scattering entities per unit incident intensity per unit solid angle [51]. The BSC is an acoustic signature of a tissue's microstructure and is therefore not dependent on the scanner and US probe sensitivity. This is a quantitative and reproducible absolute measure that is superior to B-mode echogenicity, which is only qualitative and relative.

It is now well established that the BSC for blood is modulated by the erythrocyte aggregation state that can be modified by flow or shear rate, plasma fibrinogen concentration and hematocrit  $H$  [12,37,50, 51]. By measuring blood BSC at different frequencies, it has been shown that the frequency dependence  $BSC(f)$  for non-aggregated erythrocytes obeys the Rayleigh scattering theory and its 4th power ( $f^4$ ) frequency dependence up to  $f < 30$  MHz for  $H < 30\%$  [63]. However, it has also been shown that beyond these limits, the presence of EA causes a deviation of the backscattered signal from that predicted by the Rayleigh scattering mode. By using a broadband transducer, this deviation can be quantified through the spectral analysis of  $BSC(f)$ . This approach has been extensively used in US tissue characterization to study cell apoptosis [49], for prostate cancer diagnosis [19] and to differentiate murine mammary fibroadenomas from carcinomas [40].

Our group recently introduced the Structure Factor Size Estimator (SFSE) [62], a data reduction model based on a structure factor  $S(f)$ , with the objective of solving the inverse problem, i.e., extracting blood microstructural properties from  $BSC(f)$ . This model, which assumes a known hematocrit, estimates two

physical parameters describing the microstructure of erythrocyte clusters: (1) the packing factor ( $W$ ) that increases with erythrocyte clustering and is related to the Boltzmann compressibility state equation [44], and (2) the ensemble averaged aggregate isotropic diameter ( $D$ ), a measure of the mean spatial extent of aggregates, expressed in terms of the number of erythrocytes.

### 1.2. Control of erythrocyte aggregation tendency

In order to control the aggregation tendency of erythrocytes while maintaining a consistent suspending phase, the covalent attachment of Pluronic copolymers F68 and F98 to the erythrocyte surface was employed as previously described [2]. Pluronics are block copolymers comprised of central poly(propylene glycol) chain flanked by two poly(ethylene glycol) chains. In aqueous solution, Pluronic copolymers micellize (self-aggregate) at a critical temperature dependent on the molecular weight of the poly(propylene glycol) core and copolymer concentration. By utilizing the known micellization behavior of Pluronic copolymers, following covalent attachment of derivatized Pluronic copolymers to the erythrocyte surface, it is possible to create erythrocytes with defined aggregation tendencies. Below the micellization temperature, erythrocyte aggregation is inhibited, and above the micellization temperature, erythrocyte aggregation is augmented [2].

### 1.3. Objectives

The first objective was to demonstrate that the SFSE allows characterization of EA in homogenous Couette shear flow under steady state conditions with blood at 40% hematocrit having different aggregation tendencies promoted by F68 and F98 Pluronics. The second objective was to circulate the same blood samples in the Couette instrument and a tube flow system in order to compare  $W$  and  $D$  and their dependence on the shear rate spatial pattern. The last objective was to establish the relationships between steady state bulk viscosity, measured with a low-shear viscometer, and steady state parameters  $W$  and  $D$  to extrapolate local viscosity maps in tube flow.

## 2. Material and methods

### 2.1. Blood samples

Fresh porcine blood from 4 animals was obtained from a local slaughter house. It was anticoagulated with 0.3% (w/w) EDTA. All blood samples were centrifuged (2500g for 10 min) to separate the plasma and erythrocytes. The buffy coat was carefully removed and discarded. Plasma was centrifuged at 20,000g for 20 min and platelet poor plasma (PPP) was kept to reconstitute blood with erythrocytes washed two times with phosphate buffered saline (PBS) and one more time with PPP. This high-speed centrifugation was necessary since we noted in preliminary experiments that platelet aggregates were echogenic in blood exposed to high shear ( $300 \text{ s}^{-1}$ ) in Couette flow. Hence, using PPP eliminated this confounding effect potentially affecting the interpretation of our results.

Four types of erythrocyte preparations at 40% hematocrit were then assembled: one non-aggregating erythrocytes suspended in PBS (PBS suspension), control reconstituted blood samples with erythrocytes suspended in PPP (*control*), and erythrocytes coated with tri-block copolymers termed Pluronic F68 or F98 and suspended in PPP. Briefly, the copolymer coating consisted of covalently binding a reactive succinimidyl carbonate derivative of Pluronic F68 and F98 to the primary amines on the erythrocyte

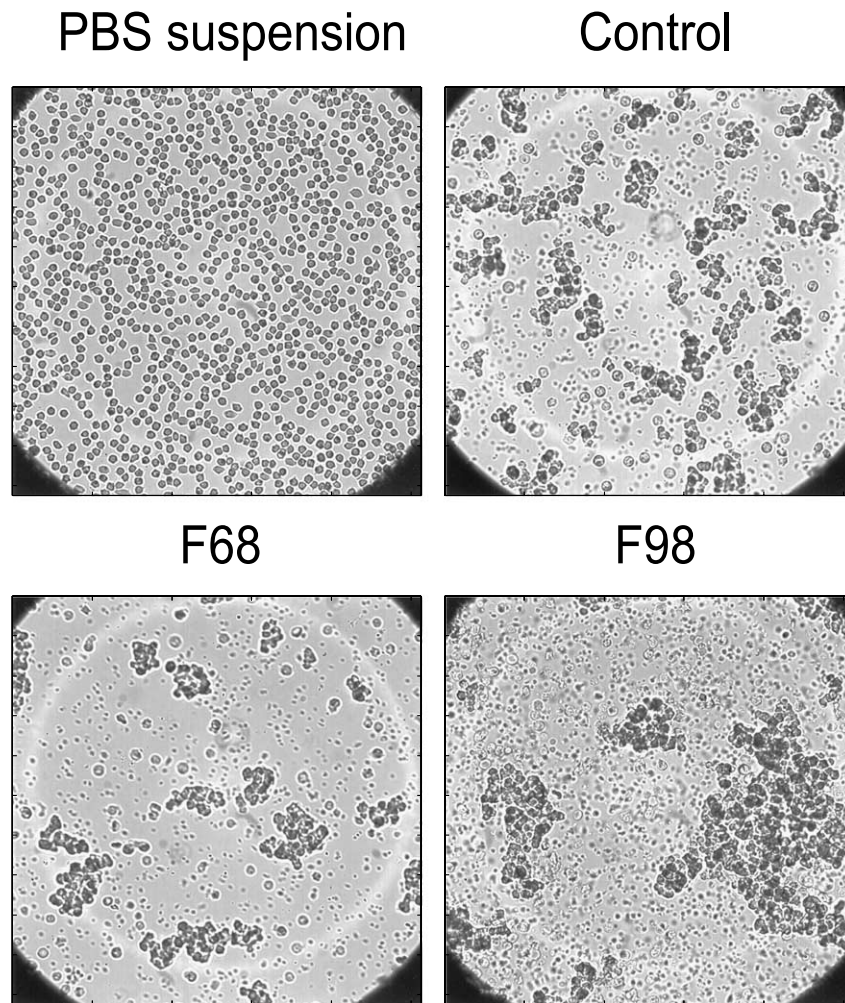


Fig. 1. Microscopic images (40 $\times$ ) of diluted ( $\approx$ 1% hematocrit) PBS suspension, *control* blood, F68 and F98 Pluronics coated erythrocytes at 25 $^{\circ}$ C. F98 increases erythrocyte aggregation whereas F68 has a neutral effect on the clustering organization.

membrane; in the present study, the concentration of the activated Pluronic during the coating process was 0.25 mg/ml of suspension. These tri-block copolymers form temperature-dependent micelles that are determined mainly by the length of the poly(propylene glycol) block chain and its concentration. At room temperature, F98 coating increases EA and F68 coating has essentially no effect on plasma-induced aggregation [2]. Figure 1 shows typical images of uncoated cells, control cells in plasma, and F68 or F98 coated cells in plasma ( $\approx$ 1% hematocrit, stasis, 25 $^{\circ}$ C). All measurements were performed at 25 $^{\circ}$ C.

## 2.2. Experimental setup

Two flow geometries were investigated in this study (see Fig. 2). A Couette flow was created between two coaxially aligned cylinders with respective diameters of 160 and 164 mm. The inner cylinder's speed was controlled using a stepper motor (Zeta 6104, Parker Hannifin Corporation, Rohnert Park, CA,

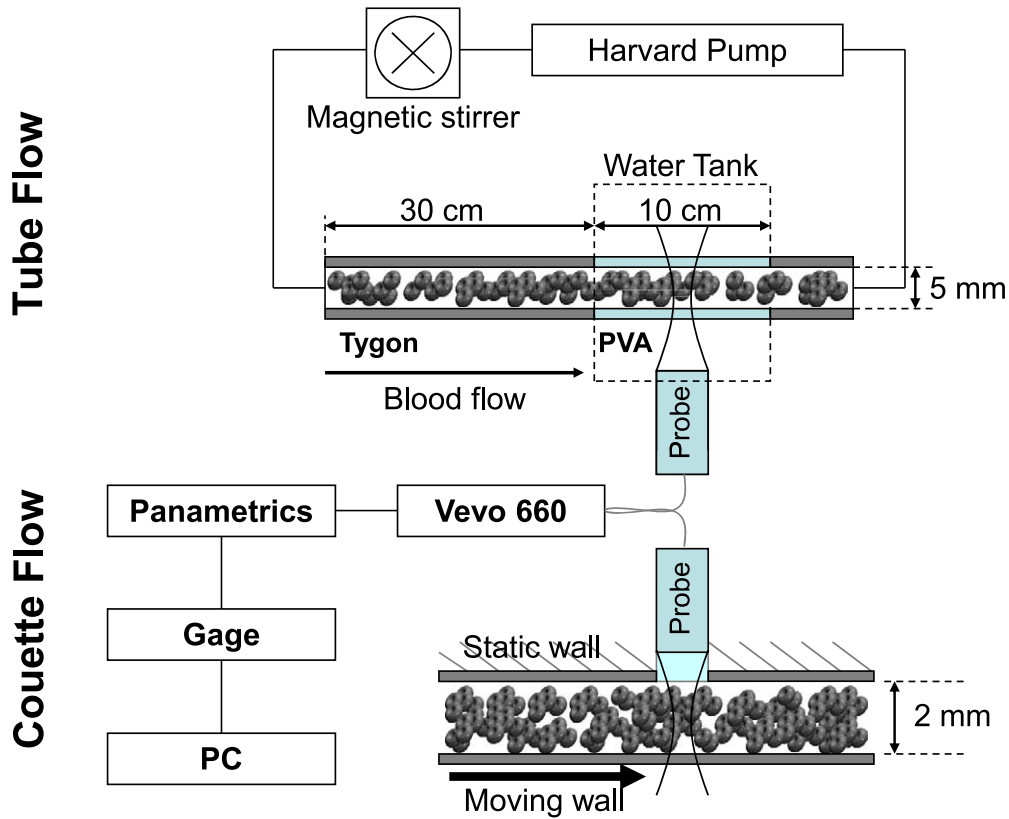


Fig. 2. Schematics of tube and Couette flow experimental setups.

USA). The ultrasound probe was positioned in the fixed outer wall of the Couette flow apparatus with its focal zone positioned at the center of the gap. The 2 mm gap was filled with 70 ml of blood, which was alternatively submitted to a disaggregating cycle of 30 s at a high-shear ( $300 \text{ s}^{-1}$ ) to initially disrupt all aggregates, and then to lower shear rates (SR) of 1, 2, 5, 10, 22, 47 and  $100 \text{ s}^{-1}$  for one minute to allow erythrocyte aggregate formation. At the one minute mark when aggregation was stabilized [62], eight ultrasound images were captured for subsequent analysis offline.

Prepared blood samples were also circulated in a horizontal straight tube submerged in degassed water at flow rates of 1, 2, 5 and  $10 \text{ ml/min}$  (5 mm inner tube diameter, 40 cm tube length). Measurements were made at 35 cm from the entrance, the required tube entry length for fully developed flow is 1.4 mm at the maximum flow rate of  $10 \text{ ml/min}$  [36], and shorter for lower flow rates. The last 10 cm section of the tube was composed of an acoustically compatible polyvinyl alcohol (PVA) cryogel tube made by applying 3 freeze-thaw cycles to the molded material [24]. A double syringe pump (model PHD2000, Harvard Apparatus, Holliston, MA, USA) was used to simultaneously push and pull blood to minimize deformation of the PVA tube. A reservoir with a magnetic stirrer was placed upstream of the tube to disaggregate erythrocyte clusters and prevent sedimentation before entering into the tube. Prior to acquiring US data, the 70 ml blood sample was moved back and forth with the Harvard pump for 10 minutes to evacuate air bubbles (which increase blood echogenicity). Blood was then flowed in the forward direction at the selected flow rate to allow aggregate formation. Twenty US images were acquired in the longitudinal

axis of the tube after one minute of steady flow to again stabilize the size of aggregates as performed for Couette flow experiments.

### 2.3. Ultrasound data acquisition and computation of the SFSE model

An ultrasound biomicroscope (Vevo 660, Visualsonics, Toronto, Canada) was used to insonify blood in B-mode with a RMV-710 probe (central frequency = 25 MHz, focal distance = 1.5 cm, F-number = 2.1), at frame rates of 5 (Couette flow) and 20 (tube flow) images/s. As the transducer was mechanically swept across the sample, sequences of RF data were amplified and filtered with a wideband acoustic receiver (model 5900 PR, Panametrics, Waltham, MA, USA), and digitized at 250 MHz with 8 bit resolution (model CS8500, Gagescope, Montreal, Canada). With these settings, one RF data block consisted of 8 or 20 images, with a pixel resolution of 21  $\mu\text{m}$  (width)  $\times$  3  $\mu\text{m}$  (depth). Each vertical line of an image was divided into overlapping segments of 400  $\mu\text{m}$  with a step resolution of 30  $\mu\text{m}$  (92.5% overlapping) for spectral estimation. This window length was determined as an acceptable compromise between image resolution and variance of power spectra.

$BSC(f)$  was computed for every position, each 400  $\mu\text{m}$  of data being Fourier transformed, averaged with corresponding segments from multiple frames and normalized across the  $-10$  dB (9–28 MHz) spectral bandwidth of the system using a 6% hematocrit reference non-aggregating erythrocyte suspension. This normalization procedure for focused transducers is known as the modified substitution method [58]. For each  $BSC(f)$ ,  $W$  and  $D$  were then calculated using the SFSE method [62]. Briefly, this data reduction model is based on a second order polynomial approximation of the structure factor  $S(f)$  that describes the weakly scattering tissue's microstructure in the spectral domain.  $S(f)$  is directly related to the pair correlation function  $g(r)$  describing spatial interactions between erythrocytes through a Fourier transform [57]. The SFSE is a minimization problem in which  $W$  and  $D$  are deduced from a polynomial fit of the measured frequency dependent  $BSC(f)$ :

$$F(W, D) = \min \|BSC(f) - m\sigma_b(f)S(f)\|^2. \quad (1)$$

In this expression,  $m$  is the scatterer number density ( $m = H/V$  with  $H$  the known hematocrit and  $V$  the volume of an erythrocyte),  $\sigma_b$  is the backscattering cross-section of an erythrocyte scatterer prototype of radius  $a$  (i.e., in the frequency range used in this study, the error on  $\sigma_b$  is about 5% when using a sphere with a volume  $V$  rather than a typical biconcave erythrocyte [47]) and  $S$  is the structure factor that is approximated by the polynomial expression [62]:

$$S(f) \approx W - \frac{12}{5} \left( \frac{2\pi}{c} \right)^2 (Da)^2 f^2. \quad (2)$$

This model considers that the increase in  $BSC(f)$  with aggregation is caused by a change in erythrocyte positions that has an effect on  $S(f)$ , both  $W$  and  $D$  increase when erythrocytes form clusters.

### 2.4. Velocity and shear rate assessments based on speckle tracking analysis

The positioning of the US probe in the longitudinal plane for both Couette and tube flow geometries allowed performing velocity speckle tracking analyses on sequences of B-mode images [56]. A cross correlation algorithm was used to find the translation of a prototype window in two successive frames across the region of interest. By measuring displacements of speckle and knowing the elapsed time

between two images, spatially varying velocities could be determined. For Couette flow, a homogeneous shear rate and a linear velocity profile were measured (data not shown), whereas for tube flow, the shear rate profile was estimated from the velocity profile determined by fitting the power law

$$v(r) = v_{\max} \left[ 1 - \left( \frac{r}{R} \right)^n \right], \quad (3)$$

where  $v_{\max}$  is the maximum velocity,  $r$  is the radial position and  $R$  the tube radius. A power law with  $n = 2$  describes a Poiseuille parabolic flow, whereas  $n$  greater than 2 indicates the blunting of the velocity profile caused by aggregation [13,48]. The shear rate  $SR(r)$  was calculated at the different radial positions using

$$SR(r) = \frac{\partial v(r)}{\partial r} = n v_{\max} \frac{r^{n-1}}{R^n}. \quad (4)$$

To simplify the data analysis of  $W$  and  $D$  as a function of the shear rate in tube flow, both indices were pooled over image areas covering different shear rate intervals. Namely, the label SR 1 was used to indicate regions with  $SR \leq 1 \text{ s}^{-1}$ , SR 2 regions with  $1 \text{ s}^{-1} < SR \leq 2 \text{ s}^{-1}$ , SR 5 regions with  $2 \text{ s}^{-1} < SR \leq 5 \text{ s}^{-1}$  and SR 10 regions with  $5 \text{ s}^{-1} < SR \leq 10 \text{ s}^{-1}$ .

### 2.5. Viscosity measurements

Viscosity measurements were performed with a low-shear viscometer (Contraves LS30, Zurich, Switzerland) at 25°C on similar pig blood samples prepared on site by Dr. J.K. Armstrong in Los Angeles. PBS suspensions, *control* blood, F68 and F98 coated erythrocytes were studied at shear rates varying from 1 to 100  $\text{s}^{-1}$ .

## 3. Results

### 3.1. Ultrasound measures in Couette flow

#### 3.1.1. BSC( $f$ ) and SFSE model

The SFSE model allowed extracting the erythrocyte aggregation parameters  $W$  and  $D$  from the spectral content of the backscattering coefficient  $BSC(f)$ . Figure 3 illustrates typical  $BSC(f)$  for the 4 blood types at selected SR of 1, 2, 5, 22 and 100  $\text{s}^{-1}$ . Experimental  $BSC(f)$  are represented by discrete points and SFSE fittings are traced in full lines. The respective values of  $W$ ,  $D$  and the correlation coefficient  $r^2$  of the fitted model are shown in the legend. In Fig. 3a for the PBS suspension,  $W$  and  $D$  were SR independent because of the absence of aggregation. With normal aggregating erythrocytes (*control* – panel b and F68 – panel c), decreasing the shear rate resulted in increases in  $W$  and  $D$ . For both types of blood, the SFSE performed very well with  $r^2$  values higher than 0.94. However, for the hyperaggregating F98-coated erythrocytes (panel d), the SFSE could not follow the frequency dependence of  $BSC(f)$  at shear rates of 2 and 5  $\text{s}^{-1}$  when  $D$  became larger than 13.7 (value at 22  $\text{s}^{-1}$ ), as reflected by drastically lower values of  $r^2$ . The frequency dependence of aggregated erythrocytes between 9 and 28 MHz could only be efficiently modeled with the SFSE when  $D < 14$ , i.e., for  $kDa < 4.3$  at  $f = 28$  MHz, where  $k$  is the acoustic wave vector defined as  $k = \frac{2\pi f}{c}$  with  $c$  the speed of sound in biological tissues ( $\approx 1540$  m/s).

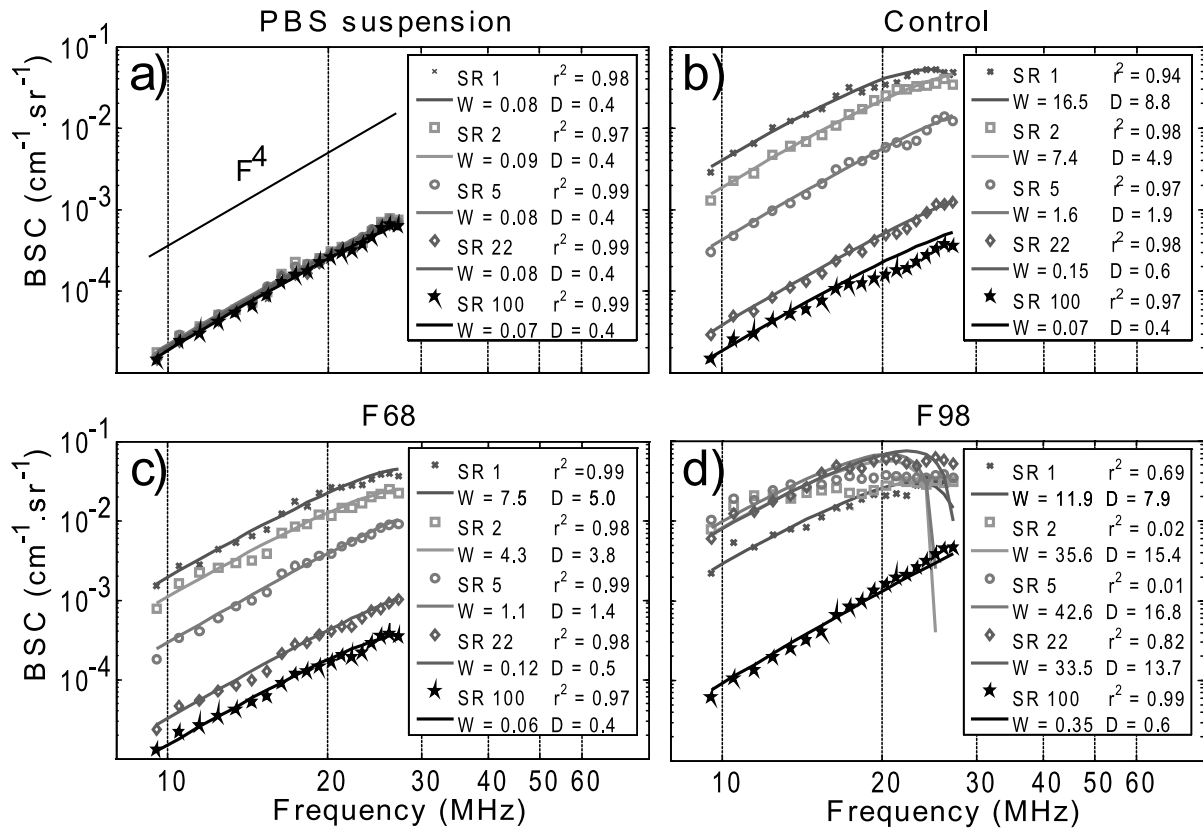


Fig. 3. Typical experimental backscatter coefficient BSC as a function of the ultrasound frequency for (a) erythrocytes suspended in PBS (no aggregation), (b) *control* blood samples, (c) F68 coated blood samples and (d) F98 hyperaggregating coated blood samples under Couette flow. Lines indicate the Structure Factor Size Estimator (SFSE) fitting of experimental data, SR is the shear rate,  $W$  and  $D$  are erythrocyte aggregation measurements, and  $r^2$  is the correlation coefficient of the fitting.

### 3.1.2. SFSE reproducibility

The reproducibility of the SFSE measurements was evaluated in the Couette homogenous shear field.  $W$  and  $D$  were computed on one control sample using 5 repetitions of the protocol at SR of 1, 2, 5, 10, 22, 47 and  $100 \text{ s}^{-1}$ . Results are presented in Fig. 4 where both  $W$  and  $D$  are seen to decrease with increasing SR. At a SR of  $100 \text{ s}^{-1}$ ,  $W$  was  $0.08 \pm 0.01$  (mean  $\pm$  SE) and  $D$  was smaller than 1 ( $0.51 \pm 0.04$ ), both values corresponding to disaggregated erythrocytes [62].  $W$  and  $D$  standard errors increased with aggregation at the lower shear rates (logarithmic scale). Statistically different levels of  $W$  and  $D$  ( $p < 0.05$ ) were found between all SR, except between 47 and  $100 \text{ s}^{-1}$  (Student–Newman–Keuls pair-wise comparisons of the mean ranks, Sigmastat 3.11, Systat Software, San Jose, CA, USA), where erythrocyte aggregation is very low or absent.

### 3.1.3. SFSE and viscosity shear rate dependencies

Shear rate dependencies of  $W$  (panel a),  $D$  (panel b) and apparent viscosity (panel c) for Couette flow are presented in Fig. 5. For the PBS suspension, these three parameters were SR independent between 1 and  $100 \text{ s}^{-1}$ . For the *control* and F68 samples, each index showed a gradual decrease with increasing SR, at any SR, values of  $W$ ,  $D$  and viscosity were similar for both types of blood. For F98, only data for  $SR \geq 47 \text{ s}^{-1}$  are presented because of the limit of the SFSE model, i.e. that it was unable to fit  $BSC(f)$  at

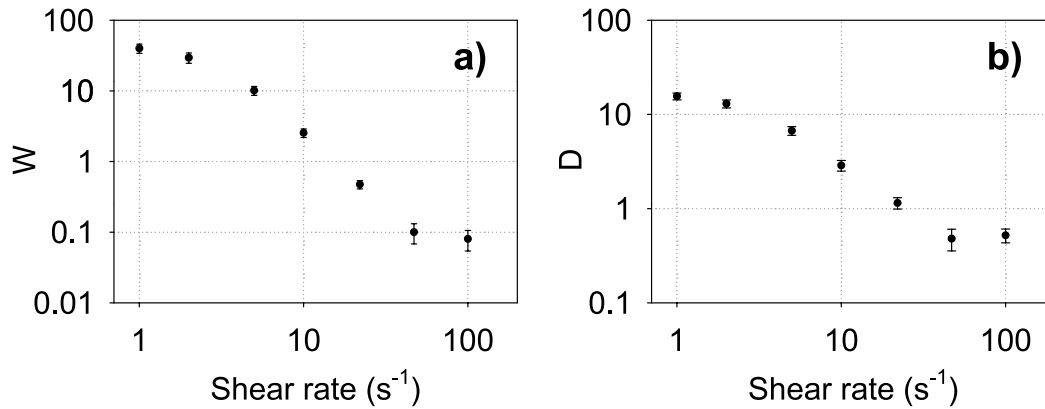


Fig. 4. (a)  $W$  and (b)  $D$  in Couette flow as a function of the shear rate for 5 measurements realized with a control blood sample. Results are mean  $\pm$  SE. Statistically different levels ( $p < 0.05$ ) of  $W$  and  $D$  were found between all SR, except between 47 and  $100 s^{-1}$ .

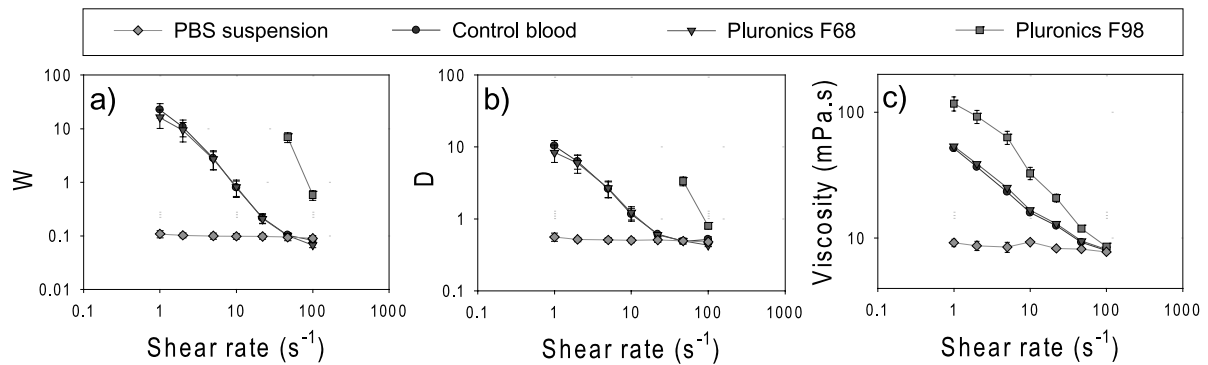


Fig. 5. Shear rate dependencies of (a)  $W$ , (b)  $D$  and (c) bulk viscosity (measured with a low shear viscometer) for the 4 blood samples (PBS suspension, *control* blood, F68 and F98 coated erythrocytes) collected from 4 animals. Results in Couette flow experiments are mean  $\pm$  SE.

lower SR. As expected, values of each rheological parameter for the F98 suspension were higher when compared with other blood types, and decreased with increasing shear rates.

Quantitative comparisons of  $W$  and  $D$  were performed between blood types using Student–Newman–Keuls pairwise statistics of the mean ranks for each SR, with  $p < 0.05$  considered to be significant. No differences were found at any SR between *control* and F68 groups or between *control*, F68 and PBS suspension at SR of 47 and  $100 s^{-1}$ . Significant differences were found between normal aggregating erythrocytes (*control* and F68) and PBS suspended cells at SR of 1, 2, 5, 10 and  $22 s^{-1}$  for  $W$  and at SR of 1, 2, 5 and  $10 s^{-1}$  for  $D$ . Finally,  $W$  and  $D$  were significantly higher for the F98 group than for all other groups.

Based upon the results shown in Fig. 5, the bulk viscosity of each blood type may be predicted by parameters  $W$  and  $D$  since all three indices varied similarly as a function of SR. Linear stepwise backward regressions were used to determine these relations, with linear regression equations and correlation coefficients for viscosity versus  $W$  and  $D$  presented in Table 1. Based on the correlation coefficients,  $D$  is a somewhat better predictor of viscosity, relations between  $D$  and viscosity are shown in Fig. 6.

Table 1  
Bulk viscosity as a function of ultrasound parameters  $D$  and  $W$

Blood sample	Linear regression equation	Correlation coefficient $r^2$	$p$
PBS suspension	$\eta = 8.6$		
Control	$\eta = 9.12 + 4.24D$	0.98	<0.001
	$\eta = 12.60 + 1.85W$	0.93	<0.001
F68	$\eta = 8.41 + 5.38D$	0.98	<0.001
	$\eta = 12.35 + 2.67W$	0.95	<0.001
F98	$\eta = 8.72 + 0.71D$	0.97	NS (0.08)
	$\eta = 9.33 + 0.23W$	0.96	NS (0.10)

Notes:  $\eta$  is the bulk viscosity (mPa s) measured in Couette flow with a low-shear blood viscometer;  $D$  is the steady state acoustically determined ensemble averaged isotropic aggregate diameter, expressed in number of erythrocytes;  $W$  is the steady state acoustically determined ensemble averaged packing factor (no unit); NS – non-significant.

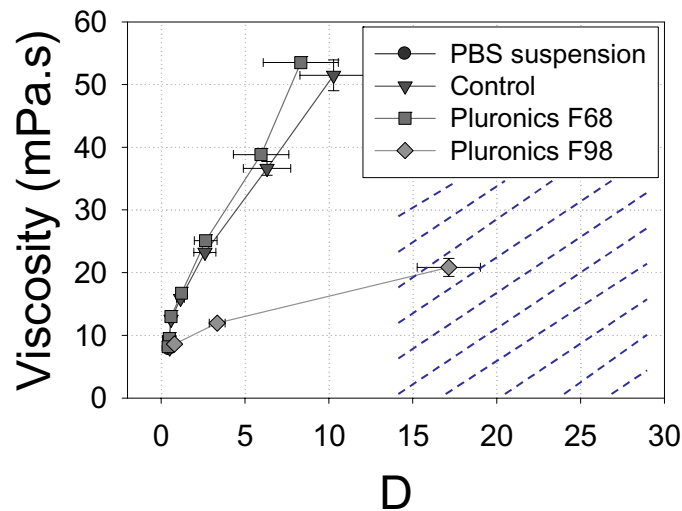


Fig. 6. Bulk viscosity as a function of the SFSE parameter  $D$  for the 4 blood types (PBS suspension, *control* blood, F68 and F98 coated erythrocytes) collected from 4 animals. Results in Couette flow experiments are mean  $\pm$  SE. The dashed section marks the limits of applicability of the SFSE model.

The linear regression for F98 did not reach significance ( $p = 0.08$ ) even when a third point at  $D \approx 17$ , which is outside the limits of applicability of the SFSE model, was utilized.

### 3.2. Ultrasound measures in tube flow

#### 3.2.1. Erythrocyte aggregation and impact on velocity and shear rate profiles

Typical velocity profiles estimated by the speckle tracking algorithm are presented in Fig. 7 for flow rates of 1, 2, 5 and 10 ml/min, also shown as upward facing lines or curves are shear rate profiles calculated using Eq. (4). For the PBS suspension (a), velocity profiles were nearly parabolic ( $n \approx 2$ ) for all shear rates. For *control* (b) and F68 (c) bloods, decreasing the flow rate provoked more blunting of velocity profiles, as reflected by monotonic increases of  $n$ . However, for F98 coated erythrocytes (d), decreasing the flow rate had the opposite effect, i.e.  $n$  decreased from 5.0 to 3.7 or 4.0 and hence less blunting occurred. As a further validation of the approach, volume integrations of velocity profiles were

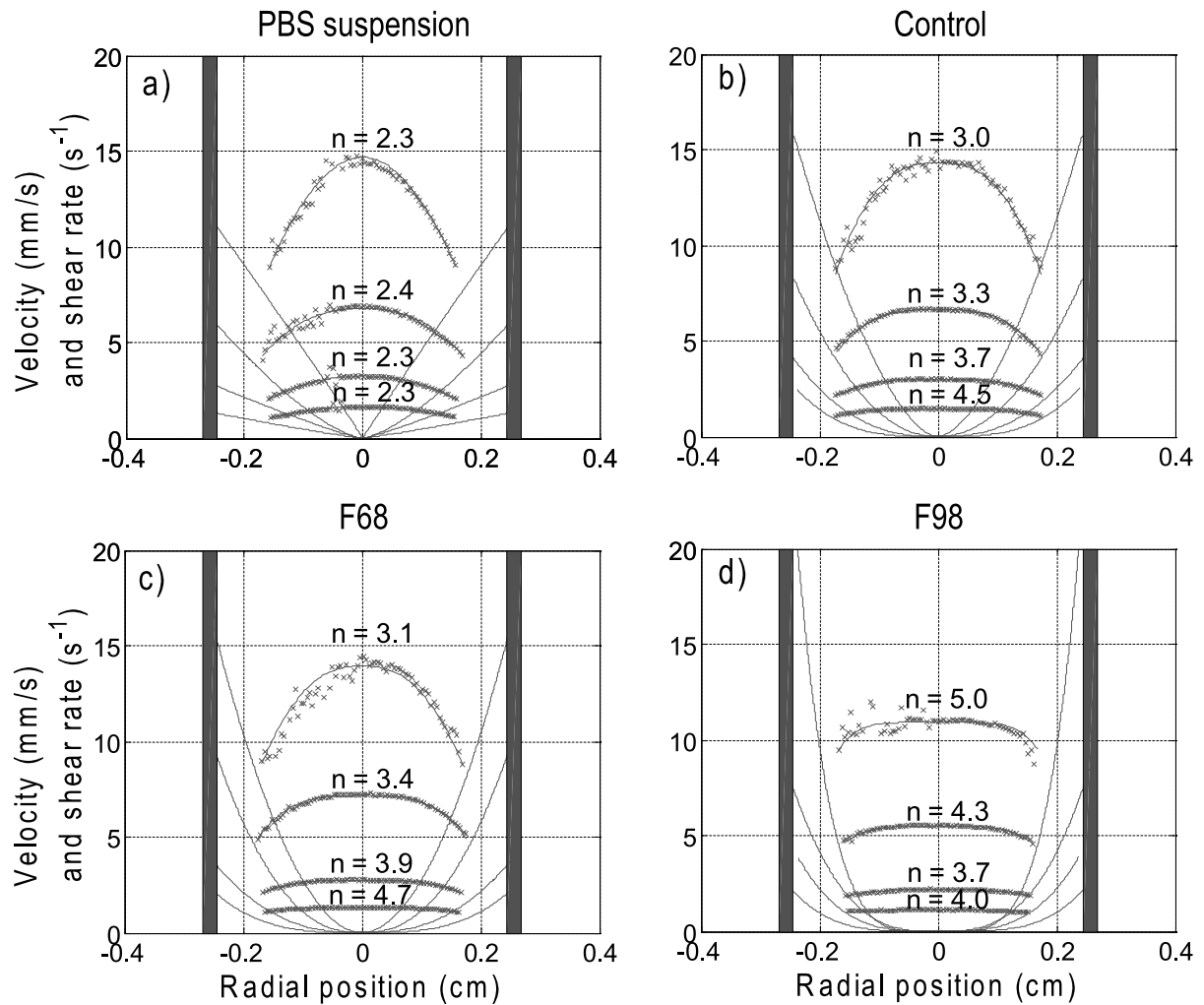


Fig. 7. Typical speckle tracking velocity results in tube flow for flow rates of 1, 2, 5 and 10 ml/min for the 4 blood types (PBS suspension, *control* blood, F68 and F98 coated erythrocytes). The shear rate profiles shown as upward facing lines or curves were deduced from Eq. (4).  $n$  is the viscosity power law exponent in Eqs (3) and (4).

compared with known flow rates of the pump in Fig. 8. The estimated flow rates were in excellent agreement for the non-aggregating PBS samples but were slightly underestimated for aggregating erythrocytes with the difference up to 10% for F98 samples.

### 3.2.2. $W$ and $D$ shear rate dependencies in tube flow

The SFSE model was applied to determine parameters  $W$  and  $D$  as in Couette flow experiments. Figure 9 presents results for *control* blood and F98 coated erythrocytes of the SR dependency of  $D$  for flow rates of 1, 2, 5 and 10 ml/min. F68 results were very similar to *control* data, whereas for the PBS suspension  $D$  was SR and flow rate independent ( $D = 0.42 \pm 0.02$ ), the SR dependency of  $W$  was similar to that for  $D$ . Note that  $D$  decreased with increasing SR and flow rates for *control* blood, whereas for F98 coated erythrocytes, the opposite was observed:  $D$  increases with increasing SR and flow rates with a similar finding for  $W$  (not shown).

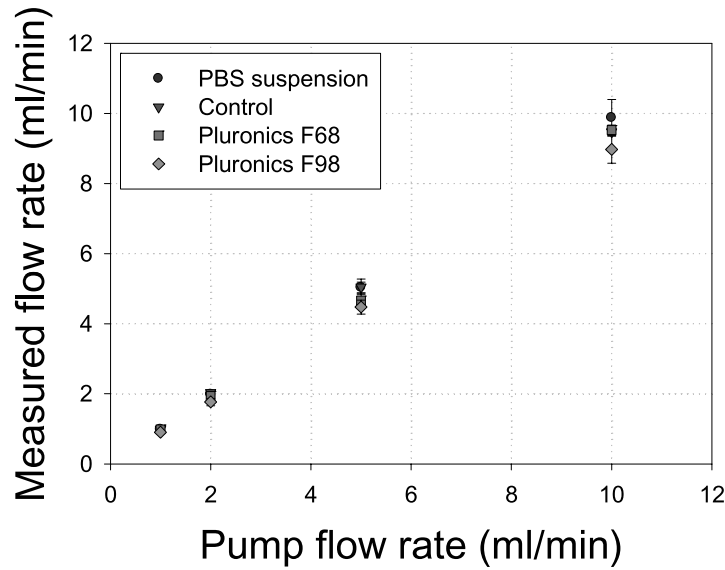


Fig. 8. Flow rate calculated from the volume integration of velocity profiles determined by speckle tracking as a function of the pump flow rate for the 4 blood types (PBS suspension, *control* blood, F68 and F98 coated erythrocytes) collected from 4 animals. Results in tube flow experiments are mean  $\pm$  SE.

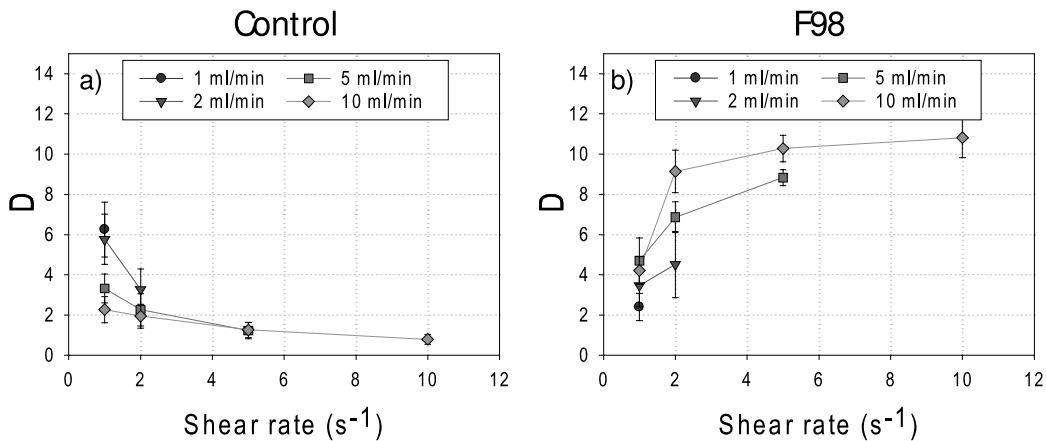


Fig. 9. Shear rate dependencies of  $D$  for (a) *control* blood and (b) F98 coated erythrocytes collected from 4 animals in tube flow rates of 1, 2, 5 and 10 ml/min. Results are mean  $\pm$  SE. Tube shear rates were calculated from speckle tracking measurements.

### 3.3. Couette and tube flow comparisons

SR dependencies of  $W$  and  $D$  in both geometries are summarized in Fig. 10. For clarity, only the tube flow rate providing the highest values of  $W$  and  $D$  at a given SR are shown (see Fig. 9). Note that the SR was varied from 1 to 100  $s^{-1}$  in Couette flow, whereas they ranged from 1 to 10  $s^{-1}$  in tube flow. With the PBS suspension,  $W$  and  $D$  were slightly lower in tube flow and were SR independent for both geometries. For *control* and F68, lower values of  $W$  and  $D$  were also noted for tube flow, but for both geometries they decreased with increasing SR as expected. Note, however, that analysis of variance (ANOVA) tests revealed no statistical difference ( $p > 0.05$ ) between both geometries at all SR for PBS,

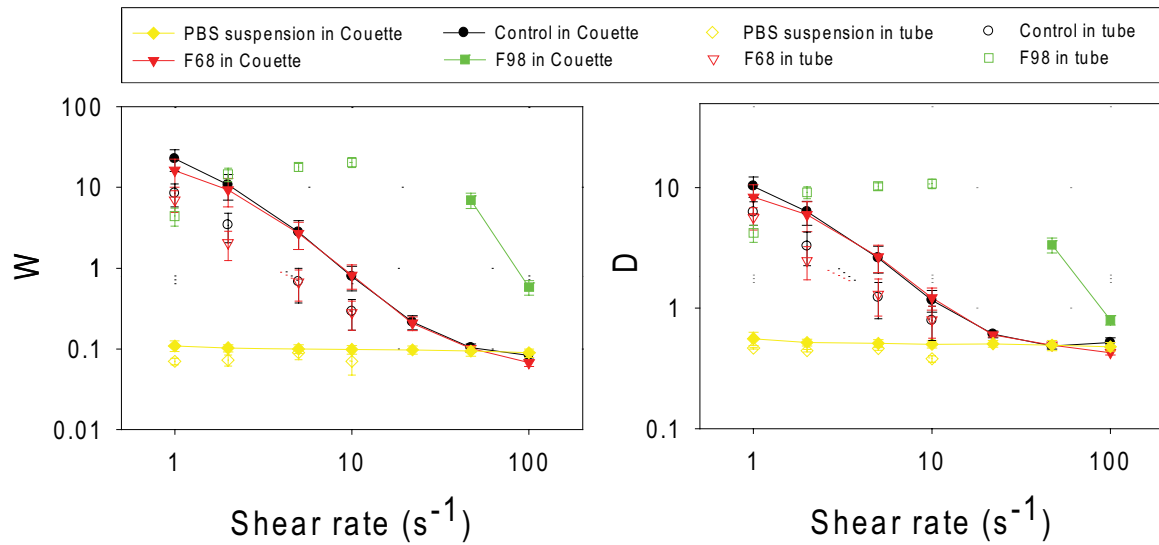


Fig. 10. Shear rate dependencies of (a)  $W$  and (b)  $D$  for the 4 blood types (PBS suspension, *control* blood, F68 and F98 coated erythrocytes) collected from 4 animals and circulated in Couette and tube flows.

*control* and F68 bloods. For F98, changes of  $W$  and  $D$  with SR were quite different (i.e., a decrease with SR in Couette flow and an increase in tube flow) but a clear comparison between both geometries was not possible because the range of SR did not overlap (Fig. 10).

### 3.4. Parametrical images of $W$ and $D$ in tube flow and viscosity predictions

Typical velocity vectors determined by speckle tracking (left column), parametric images of  $W$ ,  $D$  and predicted viscosity maps are presented for *control* (Fig. 11) and F98 (Fig. 12) bloods. In these figures, the parametric images are superimposed on a conventional B-mode frame. F68 images were very similar to *control*; PBS suspension images were spatially homogenous. The “black hole” (BH) phenomenon can be clearly seen for the *control* blood (Fig. 11) as a hypoechoic zone in the tube center of B-mode and parametric images of  $W$  and  $D$  (see below for a discussion on the BH). Large BH with less contrast than *control* blood were noted at the highest flow rates for F98 samples. For *control* blood (Fig. 11), the larger clusters of erythrocytes were concentrated in a ring located midway between the center stream and the tube wall, and corresponded to increased viscosity layers. The F98 coating also affected the radial distribution of aggregates, as illustrated in Fig. 12: at low flow rates, the effect of the F98 coating on aggregation was not very pronounced but at higher flow rates large clusters formed close to the tube walls. Interestingly, and unexpectedly, the viscosity for F98 was not markedly increased in this region (see below).

## 4. Discussion

Erythrocyte aggregation (EA) can be characterized by its effect on  $BSC(f)$  using descriptive acoustical parameters such as the ‘integrated backscatter’ (i.e., mean of the BSC intensity within the transducer frequency bandwidth) or the ‘spectral slope’ (i.e., linear regression of  $BSC(f)$  on a log–log scale) [14,35,

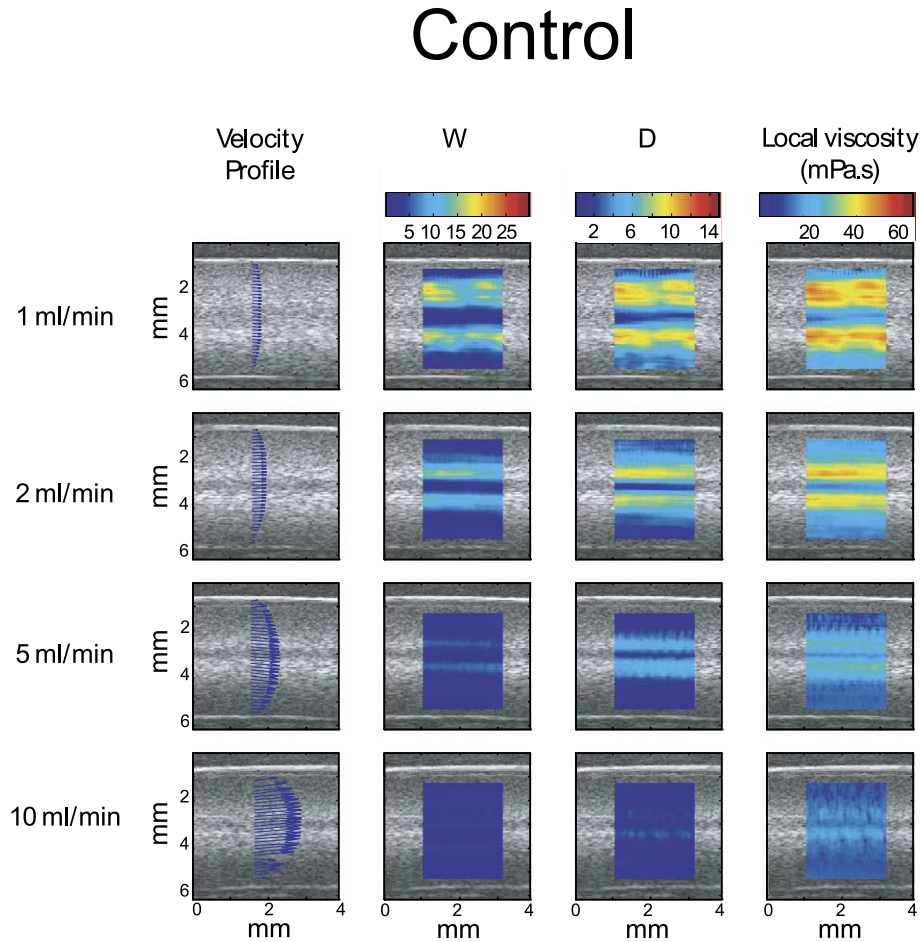


Fig. 11. Typical speckle tracking velocity vectors, parametric images of  $W$  and  $D$ , and local viscosity predictions for *control* blood in the tube flow geometry. For velocity scales, please refer to Fig. 7b where the magnitude of the velocity vectors and fitted power law profiles are represented. The “black hole” phenomenon surrounded by a bright ring can be seen in the center stream of B-mode, parametric-mode ( $W$  and  $D$ ) and viscosity images at the smallest flow rates.

58]. Indeed, the use of BSC spectral information is commonly used because such parameters are more robust than fixed frequency US intensity measurements [59]. These parameters convey information on the erythrocyte spatial organization but are inherently dependent on the frequency and transducer bandwidth, which makes comparisons between studies an arduous task. Efforts to relate acoustical parameters to blood microstructure (e.g., with the structure factor) should prove to be more robust, informative and satisfying for quantitative assessment of tissue properties.

For blood, previous attempts to relate aggregate microstructures to scattering properties have generally failed when non-Rayleigh scattering and packing effects on  $BSC(f)$  were considered. For example, the kinetics of EA after flow stoppage were quantified in a mock flow loop by concomitant increases in “effective” scatterer size and acoustic concentration (i.e., the product of scatterer concentration and squared acoustic impedance) [29] based on changes in  $BSC(f)$ . If an increase in scatterer size is coherent with aggregating erythrocytes, an increase in acoustic concentration is not as easily interpretable. Indeed, aggregation would rather decrease the number of “effective” scatterers, whereas the acoustic

## F98

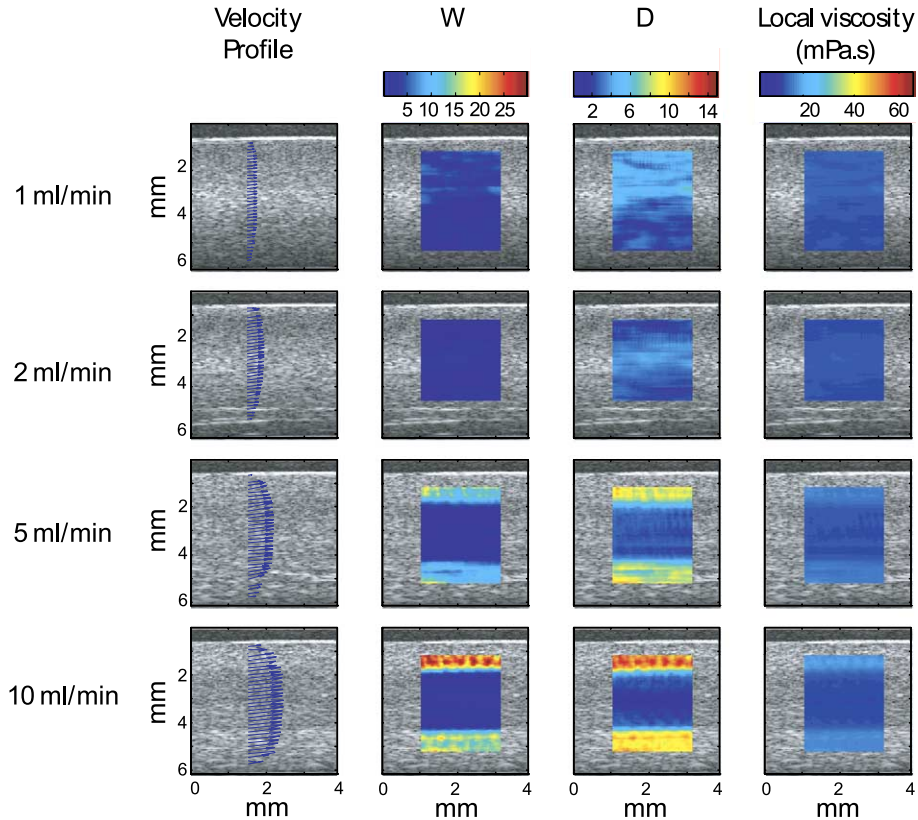


Fig. 12. Typical speckle tracking velocity vectors, parametric images of  $W$  and  $D$ , and local viscosity predictions for a hyper-aggregating F98 blood sample in the tube flow geometry. For velocity scales, please refer to Fig. 7d where the magnitude of the velocity vectors and fitted power law profiles are represented. Compared with Fig. 11, a larger “black hole” can be seen in the center stream at the highest flow rates. The bright ring is now located near the wall.

impedance would remain unchanged. The hypothesis that erythrocytes independently scatter US waves at a physiological hematocrit (e.g., 5 million erythrocytes/mm<sup>3</sup>) can be questioned for this particular model. Another model, based on the Rayleigh scattering theory, established that  $W$  was related with the local erythrocyte concentration variance [37]. Interestingly,  $W$  increased with EA but the model was limited to small aggregates with a maximum size of 4 erythrocytes [31]. With an empirical approach, also based on Rayleigh scattering, BSC dependence on hematocrit was related to the aggregate size determined by considering cell packing within aggregates and of aggregates in the suspension [6,25], but surprisingly, predicted sizes clearly exceeding Rayleigh scattering limits with aggregate sizes of up to 240 erythrocytes per aggregate.

#### 4.1. Advantages of the SFSE model

The structure factor formalism was introduced by our group to describe the effects of EA on  $BSC(f)$  in non-Rayleigh conditions for densely packed scatterers [21,22,46]. It considers that variations of  $BSC(f)$

with EA are strictly related to changes in the spatial organization of erythrocytes, considered individually as weak Rayleigh scatterers much smaller than the acoustic wavelength. The SFSE is a non-Rayleigh second-order approximation in  $f$  of the structure factor formalism that has several advantages. First, parameters  $W$  and  $D$  have a physical interpretability.  $W$  is related to the isothermal compressibility  $\xi_T$  of the tissue by  $W = mKT\xi_T$ , where  $m$  is the number density of scatterers,  $K$  the Boltzmann constant and  $T$  the absolute temperature.  $W$  is known to increase with the stickiness parameter of the analytical adhesive sphere model in a wide range of volume fractions [44]. This is also our observation with ultrasound, as  $W$  increased with aggregation, similarly to [31].  $W$  also corresponds to the analytical formulation of the packing factor in the long wavelength limit [57], when there is no aggregation, which provides a lower boundary for this parameter. This lower boundary is well understood and varies with the hematocrit. At 40% hematocrit, Perkus–Yevick approximation predicts values of  $W = 0.04$  for spheres and  $W = 0.15$  for cylinders [50]. In our experiments, we obtained  $W \approx 0.1$  for non-aggregated saline suspensions and, at high shear conditions, for aggregating erythrocytes (i.e., *control* and F68).

On the other hand, the parameter  $D$  of the SFSE model is an acoustically estimated diameter that is potentially of higher interest in hemorheology because its interpretation is easier than  $W$ . Nevertheless, its validation is difficult because, to the authors' knowledge, there is no means to experimentally assess aggregate sizes at 40% hematocrit.  $D$  is a non-dimensional number, defined as the ratio of the diameter of a fractal aggregate to the diameter of one erythrocyte, that is expected to be smaller than 1 for disaggregated erythrocytes. The apparent underestimation of the size estimate  $D$  for aggregated erythrocytes at 40% hematocrit has been previously discussed [62]. Nevertheless, in that prior publication it was shown that  $D$  was statistically correlated with the mean number of erythrocytes per aggregate, as assessed visually by microscopy at 6% hematocrit and measured acoustically at this same hematocrit.

Another advantage of the SFSE model is that  $W$  and  $D$  are parameters related to the tissue itself and should then, in theory, be independent of the frequency. In practice, because the SFSE is a second order model in  $kDa$  (see Eq. (2)), the use of a higher frequency or increased EA degrades the performance of the model. Increasing the order of the polynomial approximation of  $BSC(f)$  could theoretically extend the  $kDa$  range of applicability, but unfortunately it introduces instability in the minimization fitting algorithm. Hence the following frequency tradeoff had to be considered: (1) a larger bandwidth results in better  $W$  and  $D$  estimates, evidenced by a smaller variance, because more data are used for the polynomial fitting; (2) however, when  $W$  and  $D$  increase with aggregation, the  $kDa$  product also increases and the second order model reaches its limits of applicability, resulting in  $r^2$  dropping for the curve fitting of  $BSC(f)$  and introducing important underestimation biases of  $W$  and  $D$ . This limit occurred for  $D > 14$  for the frequency range considered in this study (9–28 MHz). By decreasing the upper frequency limit from 28 to 15 MHz for large aggregates in the F98 samples corrected this issue (data not shown) but introduced more variance in estimating smaller aggregates. Therefore, the frequency bandwidth to use must be appropriate for the levels of aggregation that are being characterized, this frequency range can be tested using  $r^2$  (see Fig. 3). Note that for clarity, in this report the bandwidth was kept constant for all results thus limiting the applicability of the SFSE to  $D < 14$ .

#### 4.2. Steady state Couette flow relationships between $D$ and measured viscosities

Multiple linear regressions showed that  $W$  and  $D$  were collinear and that  $D$  was linearly related with the bulk viscosity. Regressions in Table 1 suggested that the shear rate dependent viscosity was explained by the high shear viscosity and a multiple or fraction of  $D$ . The Flory–Fox theory [20] predicts viscosity proportional to the volume of spherical particles in suspension. The finding that the viscosity

was proportional to a multiple or fraction of  $D$  is surprising and not fully understood. It is not clear to what extent the Flory–Fox theory for colloidal suspensions can be directly applied to dense fluid deformable corpuscles, such as erythrocytes. It seems reasonable to believe that erythrocyte deformation, interacting fractal clusters and their orientation should modify the Flory–Fox relation.

Another surprising result is that the multiplicative coefficient of  $D$  for F98 samples was almost six times smaller than for the other samples (see Fig. 6). Although the linear regression did not reach statistical significance ( $p = 0.08$ , see Table 1), the tendency of the slope for the F98 sample was nevertheless clearly smaller. Since higher shear rates were required to obtain similar  $D$  values with the F98 sample, it can be speculated that the aggregate morphology was extended, thus provoking a lower viscosity versus size relation; validation of this hypothesis requires future studies.

#### 4.3. Parametrical images in tube flow

The objectives of the tube experiments were to illustrate the performance of the SFSE in a non-homogenous shear field. The presence of the BH in tube flow images illustrates the unique imaging potential of US to become a rheological tool with spatial resolution and sensitivity to EA. The BH was studied by different teams [38,41,48,64] and it is now generally accepted that it is the result of a transient state of aggregation in the center stream that is dependent on the tube entry length. Indeed, the blood flowing in the center, in the low shear region, travels in the tube more quickly and has less time to form aggregates than blood on a peripheral layer. This phenomenon is also amplified by the presence of a non-zero shear on peripheral layers that promotes aggregate formation by increasing the collision frequency between erythrocytes [16]. This aggregation kinetics related effect was still present after 3 minutes of shearing in a Couette flow for zero shear conditions, as reported previously (see Figs 2 and 3 in [62]). When clustering erythrocytes are insonified by the US probe, aggregates in the center may not have sufficient time to reach an equilibrium size as predicted by the local SR, velocity and probe position along the vessel.

The non-linear hematocrit dependence of the BSC was also suggested to explain the BH phenomenon. A decrease in  $H$  in the center axis was proposed by Yuan and Shung [64] based on the “tubular pinch” or “Segré–Silberberg” effect [7]. This behavior for fluid-like deformable corpuscles seems improbable based on earlier reports [55]: erythrocytes are rather concentrated near the center axis in that particular report. On the other hand, a local increase in hematocrit in the center axis due to erythrocyte migration towards the vessel center could provoke a decrease in BSC that may not necessarily correlate with a decrease in aggregate size. Using magnetic resonance imaging, shear rate variations in the gap of a large core Couette instrument were shown to induce migration of erythrocytes away from the walls [15], but the hematocrit variations in the center of the gap remained marginal (a few percent hematocrit). Note that a small core Couette device was used here, which should result in even smaller hematocrit variations in our data. In another magnetic resonance study, hematocrit spatial variations were shown to be non significant in tube flow [38]. Nevertheless, in a separate experiment, a 50% hematocrit hyperaggregating blood sample was prepared and sheared at  $2 \text{ s}^{-1}$  in our Couette apparatus to provide additional evidence that hematocrit changes could not explain our results. Expected high values of  $W = 15$  and  $D = 9$  were found. This illustrates that the SFSE could detect aggregation at an increased hematocrit. Also, if parameter  $H$ , an input in our model, is locally higher as it may be the case in the center stream, the SFSE would tend to overestimate  $W$  and  $D$  (data not shown). Moreover, an increase in  $H$  or EA in the center stream would cause a decrease in the spectral slope [35] and thus an increase in  $D$  that was not observed in our data. These results suggest that if hematocrit variations are present in the tube, such effects cannot

fully explain the BH. Spectral analysis of our data thus support a dominant low EA hypothesis due to very low shears and time-dependent transient effects, as clearly shown in Fig. 9a: at a given shear rate, the smallest flow rates promoted the largest aggregates. This also explains why  $W$  and  $D$  in tube flow were lower than the steady state Couette flow results in Fig. 10.

Another interesting but at a first glance unexpected observation was the increase in  $W$  and  $D$  with increasing SR for the F98 tube flow experiments (Figs 9b and 10), since for these suspensions, a SR increase promoted aggregate formation. Note that this effect was observed in another study [1] when horse blood, which is also characterized by very intense aggregation tendencies, was circulated in a tube flow setup. The mechanism explaining this phenomenon may be that more SR-induced collisions between erythrocytes are necessary to promote aggregation of cells with a high tendency to aggregate. However, as with other types of erythrocyte suspensions, disaggregation occurred with further increased the SR beyond the value inducing the maximum aggregation (see Fig. 10, Couette and tube flow data).

The low aggregation and progressive increase in  $W$  and  $D$  as the flow rate (shear rate) was increased can be visualized in Fig. 12 for F98 samples. This figure also shows that the maximum selected flow rate of 10 ml/min was not sufficient to induce erythrocyte disaggregation close to the tube wall, where the shear rate was maximum. Disaggregation was nonetheless noted close to the wall for *control* samples as the flow rate was increased (see Fig. 11). Interestingly, and of potential rheological and pathophysiological impact, is the observation of a ring with large aggregates close to the wall at the highest flow rates of 5 and 10 ml/min for F98 samples (Fig. 12), and a depleted ring with few or no aggregates close to the wall for *control* samples regardless of the flow rate (Fig. 11). For hyperaggregating erythrocytes such as F98 samples, the presence of high EA close to the wall could influence blood/vessel wall interactions.

As discussed earlier when interpreting results of Figs 5 and 6, the viscosity maps of Fig. 12 for F98 samples did not reflect the increased EA close to the wall as the flow rate was increased. The lower slope of the viscosity versus  $D$  and  $W$  relations for the Couette experiments of Fig. 6 can explain this observation. Likely, as mentioned before, the lower SR in tube flow ( $SR < 22 \text{ s}^{-1}$  at all flow rates, see Fig. 7d) compared with Couette flow, where SR were varied from 47 to  $100 \text{ s}^{-1}$ , may have biased (i.e., underestimated) the prediction. The steady state Couette flow relation between viscosity and  $D$  that we used in our predictions of Fig. 12 and also Fig. 11 were based on the hypothesis that the increase in bulk viscosity was directly caused by an increase in aggregate size. Any consideration affecting the viscosity versus particle size relation, such as deformability, erythrocyte cluster orientation or elongation with increased flow, could not be accounted for in this simplistic approach.

#### 4.4. Towards an *in vivo* assessment of the pathological impact of erythrocyte hyperaggregation

If the hematocrit is known, we have shown that precise and reproducible ultrasonic structure parameters,  $W$  and  $D$ , can be obtained with the SFSE model when an adequate US frequency bandwidth is available. *In vivo*, the attenuation of the pressure wave by intervening tissues such as skin, fat and vessel wall is a major difficulty that must be overcome. It is notable that the SFSE framework was used in a minimization routine called the Structure Factor Size and Attenuation Estimator (SFSAE) and allowed the simultaneous estimation of the attenuation of different phantom layers positioned between the US probe to study erythrocyte aggregates [23]. This approach could therefore potentially be used to characterize blood microstructure through the skin *in vivo*, although further validation is still needed.

The pathophysiological impact of erythrocyte hyperaggregation has been studied by transfusion of Pluronics coated erythrocytes by members of our group [5,60]. In the current study, it was shown that F98 coated pig erythrocytes exhibited increased clustering up to shear rates as high as  $100 \text{ s}^{-1}$ . The

presence of aggregation near the tube walls was quantified with US parametrical imaging *in situ*. The natural next step would be to locally measure EA *in vivo* using ultrasound and quantify the physiological effect of increasing the aggregability using Pluronics coatings.

## 5. Conclusions

It was demonstrated in this study that the SFSE, an US non-Rayleigh scattering model, could adequately characterize EA for non-aggregating, aggregating and Pluronics coated erythrocytes. Two parameters, the packing factor ( $W$ ) and ensemble averaged aggregate isotropic diameter ( $D$ ), were compared in Couette and tube flows and predictably quantified EA with respect to SR and to blood type for  $D < 14$ . In Couette flow, empirical blood type dependent relationships between  $D$  and viscosity were established. These relationships were then used to extrapolate local viscosity maps in tube flow. In tube flow, a “black hole” (BH) appeared for aggregating bloods under some flow conditions. Analysis of the backscattered spectral information with the SFSE model supported the hypothesis that the BH originates from a time related lower aggregation in the center stream. Increasing the aggregation tendency of erythrocytes (F98 blood) resulted in the presence of bigger aggregates near the walls at the highest flow rates (aggregates were present at shear rates up to  $100 \text{ s}^{-1}$  in Couette flow). Preliminary results also suggested that in near stasis conditions, a higher shear rate was necessary to promote aggregate formation with the F98 samples, resulting in larger BH. The *in vivo* significance of the BH remains to be established. Parametrical images, superimposed on B-mode displays, clearly illustrated the unique capacity of ultrasound to reveal spatially non-homogenous EA states. Ultrasound opens new perspectives for *in vivo* macrocirculatory studies on the impact of hemodynamic perturbations and complications caused by EA using high frequency US, which can be locally monitored and characterized non invasively through the skin *in vivo* and *in situ*.

## Acknowledgements

Supported by grants from the Canadian Institutes of Health Research (#MOP-84358 and #CMI-72323), Heart and Stroke Foundation of Canada (#PG-05-0313), National Institutes of Health of USA (#R01HL078655) and Natural Sciences and Engineering Research Council of Canada Ph.D. scholarship program (#ES D3-317051-2005).

## References

- [1] L. Allard and G. Cloutier, Power Doppler ultrasound scan imaging of the level of red blood cell aggregation: An *in vitro* study, *J. Vasc. Surg.* **30** (1999), 157–168.
- [2] J.K. Armstrong, H.J. Meiselman, R.B. Wenby and T.C. Fisher, Modulation of red blood cell aggregation and blood viscosity by the covalent attachment of Pluronic copolymers, *Biorheology* **38** (2001), 239–247.
- [3] J.K. Armstrong, R.B. Wenby, H.J. Meiselman and T.C. Fisher, The hydrodynamic radii of macromolecules and their effect on red blood cell aggregation, *Biophys. J.* **87** (2004), 4259–4270.
- [4] P. Bagchi, P.C. Johnson and A.S. Popel, Computational fluid dynamic simulation of aggregation of deformable cells in a shear flow, *J. Biomech. Eng.* **127** (2005), 1070–1080.
- [5] O.K. Baskurt, O. Yalcin, S. Ozdem, J.K. Armstrong and H.J. Meiselman, Modulation of endothelial nitric oxide synthase expression by red blood cell aggregation, *Am. J. Physiol. Heart Circ. Physiol.* **286** (2004), H222–H229.
- [6] M. Boynard and J.C. Lelièvre, Size determination of red blood cell aggregates induced by dextran using ultrasound backscattering phenomenon, *Biorheology* **27** (1990), 39–46.

- [7] C.G. Caro, T.J. Pedley, R.C. Schroter and W.A. Seed, *The Mechanics of the Circulation*, 1st edn, Oxford University Press, Toronto, 1978, pp. 1–514.
- [8] S. Chien, Blood viscosity: Influence of erythrocyte aggregation, *Science* **157** (1967), 829–831.
- [9] S. Chien, Biophysical behavior of red cells in suspensions, in: *The Red Blood Cell*, D.M. Surgenor, ed., Academic Press, New York, 1975, pp. 1031–1133.
- [10] S.C. Christiansen, S.C. Cannegieter, T. Koster, J.P. Vandenbroucke and F.R. Rosendaal, Thrombophilia, clinical factors, and recurrent venous thrombotic events, *JAMA* **293** (2005), 2352–2361.
- [11] G. Cloutier, M. Daronat, D. Savéry, D. Garcia et al., Non-Gaussian statistics and temporal variations of the ultrasound signal backscattered by blood at frequencies between 10 and 58 MHz, *J. Acoust. Soc. Am.* **116** (2004), 566–577.
- [12] G. Cloutier and Z. Qin, Ultrasound backscattering from non-aggregating and aggregating erythrocytes – A review, *Biorheology* **34** (1997), 443–470.
- [13] G. Cloutier and Z. Qin, Shear rate dependence of ultrasound backscattering from blood samples characterized by different levels of erythrocyte aggregation, *Ann. Biomed. Eng.* **28** (2000), 399–407.
- [14] G. Cloutier, A. Zimmer, F.T. Yu and J.L. Chiasson, Increased shear rate resistance and fastest kinetics of erythrocyte aggregation in diabetes measured with ultrasound, *Diabet. Care* **31** (2008), 1400–1402.
- [15] G.R. Cokelet, J.R. Brown, S.L. Codd and J.D. Seymour, Magnetic resonance microscopy determined velocity and hematocrit distributions in a Couette viscometer, *Biorheology* **42** (2005), 385–399.
- [16] A.L. Copley, R.G. King and C.R. Huang, Erythrocyte sedimentation of human blood at varying shear rates, in: *Microcirculation*, J. Grayson and W. Zingg, eds, Plenum Press, New York, 1976, pp. 133–134.
- [17] M.G.M. de Kroon, C.J. Slager, W.J. Gussenhoven, P.W. Serruys et al., Cyclic changes of blood echogenicity in high-frequency ultrasound, *Ultrasound Med. Biol.* **17** (1991), 723–728.
- [18] J. Fang and R.G. Owens, Numerical simulations of pulsatile blood flow using a new constitutive model, *Biorheology* **43** (2006), 637–660.
- [19] E.J. Feleppa, C.R. Porter, J. Ketterling, P. Lee et al., Recent developments in tissue-type imaging (TTI) for planning and monitoring treatment of prostate cancer, *Ultrason. Imaging* **26** (2004), 163–172.
- [20] P.J. Flory and T.G.J. Fox, Treatment of intrinsic viscosity, *J. Am. Chem. Soc.* **73** (1951), 1904–1906.
- [21] I. Fontaine, M. Bertrand and G. Cloutier, A system-based approach to modeling the ultrasound signal backscattered by red blood cells, *Biophys. J.* **77** (1999), 2387–2399.
- [22] I. Fontaine, D. Savéry and G. Cloutier, Simulation of ultrasound backscattering by red cell aggregates: Effect of shear rate and anisotropy, *Biophys. J.* **82** (2002), 1696–1710.
- [23] E. Franceschini, F.T.H. Yu and G. Cloutier, Simultaneous estimation of attenuation and structure parameters of aggregated red blood cells from backscatter measurements, *J. Acoust. Soc. Am.* **123** (2008), EL85–EL91.
- [24] J. Fromageau, J.L. Gennisson, C. Schmitt, R.L. Maurice et al., Estimation of polyvinyl alcohol cryogel mechanical properties with 4 ultrasound elastography methods and comparison with gold standard testings, *IEEE Trans. Ultrason. Ferroelectr. Freq. Control* **54** (2007), 498–509.
- [25] M. Hanss and M. Boynard, Ultrasound backscattering from blood: Hematocrit and erythrocyte aggregation dependence, in: *Ultrasonic Tissue Characterization II*, M. Linzer, ed., National Bureau of Standards, Gaithersburg, MD, 1979, pp. 165–169.
- [26] B.M. Johnston, P.R. Johnston, S. Corney and D. Kilpatrick, Non-Newtonian blood flow in human right coronary arteries: transient simulations, *J. Biomech.* **39** (2006), 1116–1128.
- [27] T. Khodabandehlou and C. Le Devehat, Hemorheological disturbances as a marker of diabetic foot syndrome deterioration, *Clin. Hemorheol. Microcirc.* **30** (2004), 219–223.
- [28] H. Kitamura and S. Kawasaki, Detection and clinical significance of red cell aggregation in the human subcutaneous vein using a high-frequency transducer (10 MHz): A preliminary report, *Ultrasound Med. Biol.* **23** (1997), 933–938.
- [29] H. Kitamura, B. Sigel, J. Machi, E.J. Feleppa et al., Roles of hematocrit and fibrinogen in red cell aggregation determined by ultrasonic scattering properties, *Ultrasound Med. Biol.* **21** (1995), 827–832.
- [30] E. Krieger, B. van Der, Loo, B.R. Amann-Vesti, V. Rousson and R. Koppensteiner, C-reactive protein and red cell aggregation correlate with late venous function after acute deep venous thrombosis, *J. Vasc. Surg.* **40** (2004), 644–649.
- [31] B. Lim and R.S. Cobbold, On the relation between aggregation, packing and the backscattered ultrasound signal for whole blood, *Ultrasound Med. Biol.* **25** (1999), 1395–1405.
- [32] G.D.O. Lowe, A.J. Lee, A. Rumley, J.F. Price et al., Blood viscosity and risk of cardiovascular events: the Edinburgh artery study, *Br. J. Haematol.* **96** (1997), 168–173.
- [33] S.M. MacRury, S.E. Lennie, P. McColl, R. Balendra et al., Increased red cell aggregation in diabetes mellitus: Association with cardiovascular risk factors, *Diabet. Med.* **10** (1993), 21–26.
- [34] E.L. Madsen, M.F. Insana and J.A. Zagzebski, Method of data reduction for accurate determination of acoustic backscatter coefficients, *J. Acoust. Soc. Am.* **76** (1984), 913–923.
- [35] S. Maruvada, K.K. Shung and S. Wang, High-frequency backscatterer and attenuation measurements of porcine erythrocyte suspensions between 30–90 MHz, *Ultrasound Med. Biol.* **28** (2002), 1081–1088.

- [36] W.R. Milnor, *Hemodynamics*, 2nd edn, Williams & Wilkins, Baltimore, MD, 1989, pp. 1–387.
- [37] L.Y.L. Mo and R.S.C. Cobbold, Theoretical models of ultrasonic scattering in blood, in: *Ultrasonic Scattering in Biological Tissues*, K.K. Shung and G.A. Thieme, eds, CRC Press, Boca Raton, FL, 1993, pp. 125–170.
- [38] L.Y.L. Mo, G. Yip, R.S.C. Cobbold, C. Gutt et al., Non-Newtonian behavior of whole blood in a large diameter tube, *Biorheology* **28** (1991), 421–427.
- [39] L.C. Nguyen, F.T. Yu and G. Cloutier, Cyclic changes in blood echogenicity under pulsatile flow are frequency dependent, *Ultrasound Med. Biol.* **34** (2008), 664–673.
- [40] M.L. Oelze, W.D. O'Brien Jr., J.P. Blue and J.F. Zachary, Differentiation and characterization of rat mammary fibroadenomas and 4T1 mouse carcinomas using quantitative ultrasound imaging, *IEEE Trans. Med. Imaging* **23** (2004), 764–771.
- [41] Z. Qin, L.G. Durand and G. Cloutier, Kinetics of the “black hole” phenomenon in ultrasound backscattering measurements with red blood cell aggregation, *Ultrasound Med. Biol.* **24** (1998), 245–256.
- [42] D. Quemada, Towards a unified model of elasto-thixotropy of biofluids, *Biorheology* **21** (1984), 423–436.
- [43] M.W. Rampling, H.J. Meiselman, B. Neu and O.K. Baskurt, Influence of cell-specific factors on red blood cell aggregation, *Biorheology* **41** (2004), 91–112.
- [44] C. Regnaut and J.C. Ravey, Application of the adhesive sphere model to the structure of colloidal suspensions, *J. Chem. Phys.* **91** (1989), 1211–1221.
- [45] P. Riha, M. Donner and J.F. Stoltz, Time-dependent formation of red blood cell aggregates and its influence on blood rheological behaviour, *J. Biol. Phys.* **19** (1993), 65–70.
- [46] D. Savéry and G. Cloutier, A point process approach to assess the frequency dependence of ultrasound backscattering by aggregating red blood cells, *J. Acoust. Soc. Am.* **110** (2001), 3252–3262.
- [47] D. Savéry and G. Cloutier, High-frequency ultrasound backscattering by blood: analytical and semianalytical models of the erythrocyte cross section, *J. Acoust. Soc. Am.* **121** (2007), 3963–3971.
- [48] R.E.N. Shehada, R.S.C. Cobbold and L.Y.L. Mo, Aggregation effects in whole blood: Influence of time and shear rate measured using ultrasound, *Biorheology* **31** (1994), 115–135.
- [49] M.D. Sherar, M.B. Noss and F.S. Foster, Ultrasound backscatter microscopy images the internal structure of living tumour spheroids, *Nature* **330** (1987), 493–495.
- [50] K.K. Shung, On the ultrasound scattering from blood as a function of hematocrit, *IEEE Trans. Sonics Ultrasonics* **29** (1982), 327–331.
- [51] K.K. Shung, R.A. Sigelmann and J.M. Reid, Scattering of ultrasound by blood, *IEEE Trans. Biomed. Eng.* **23** (1976), 460–467.
- [52] B. Sigel, J. Machi, J.C. Beitler, J.R. Justin and J.C.U. Coelho, Variable ultrasound echogenicity in flowing blood, *Science* **218** (1982), 1321–1323.
- [53] R.A. Sigelmann and J.M. Reid, Analysis and measurement of ultrasound backscattering from an ensemble of scatterers excited by sine-wave bursts, *J. Acoust. Soc. Am.* **53** (1973), 1351–1355.
- [54] J.F. Stoltz and M. Donner, Red blood cell aggregation: Measurements and clinical applications, *Tr. J. Med. Sci.* **15** (1991), 26–39.
- [55] S. Swarnamani and M. Singh, Analysis of erythrocyte aggregation mechanism in presence of dextran and magnetic field by ultrasound scattering in blood, *Biorheology* **26** (1989), 847–862.
- [56] G.E. Trahey, J.W. Allison and O.T. von Ramm, Angle independent ultrasonic detection of blood flow, *IEEE Trans. Biomed. Eng.* **34** (1987), 965–967.
- [57] V. Twersky, Low-frequency scattering by correlated distributions of randomly oriented particles, *J. Acoust. Soc. Am.* **81** (1987), 1609–1618.
- [58] S.H. Wang and K.K. Shung, An approach for measuring ultrasonic backscattering from biological tissues with focused transducers, *IEEE Trans. Biomed. Eng.* **44** (1997), 549–554.
- [59] K.A. Wear, T.A. Stiles, G.R. Frank, E.L. Madsen et al., Interlaboratory comparison of ultrasonic backscatter coefficient measurements from 2 to 9 MHz, *J. Ultrasound Med.* **24** (2005), 1235–1250.
- [60] O. Yalcin, F. Aydin, P. Ulker, M. Uyklu et al., Effects of red blood cell aggregation on myocardial hematocrit gradient using two approaches to increase aggregation, *Am. J. Physiol. Heart Circ. Physiol.* **290** (2006), H765–H771.
- [61] J.W. Yarnell, I.A. Baker, P.M. Sweetnam, D. Bainton et al., Fibrinogen, viscosity, and white blood cell count are major risk factors for ischemic heart disease. The Caerphilly and Speedwell collaborative heart disease studies, *Circulation* **83** (1991), 836–844.
- [62] F.T.H. Yu and G. Cloutier, Experimental ultrasound characterization of red blood cell aggregation using the structure factor size estimator, *J. Acoust. Soc. Am.* **122** (2007), 645–656.
- [63] Y.W. Yuan and K.K. Shung, Ultrasonic backscatter from flowing whole blood. II: Dependence on frequency and fibrinogen concentration, *J. Acoust. Soc. Am.* **84** (1988), 1195–1200.
- [64] Y.W. Yuan and K.K. Shung, Echoicity of whole blood, *J. Ultrasound Med.* **8** (1989), 425–434.
- [65] J. Zhang, P.C. Johnson and A.S. Popel, Red blood cell aggregation and dissociation in shear flows simulated by lattice Boltzmann method, *J. Biomech.* **41** (2008), 47–55.